





RESEARCH ARTICLE

Separations: Materials, Devices and Processes

Porous materials with suitable pore size and dual-functional sites for benchmark one-step ethylene purification

Tangyin Wu¹ | Cong Yu¹ | Rajamani Krishna²  | Zhensong Qiu¹ |
Hanqian Pan¹ | Peixin Zhang¹ | Xian Suo³ | Lifeng Yang¹  | Xili Cui^{1,3}  |
Huabin Xing^{1,3} 

¹Key Laboratory of Biomass Chemical Engineering of Ministry of Education, College of Chemical and Biological Engineering, Zhejiang University, Hangzhou, China

²Van't Hoff Institute for Molecular Sciences, University of Amsterdam, Amsterdam, The Netherlands

³Engineering Research Center of Functional Materials Intelligent Manufacturing of Zhejiang Province, ZJU-Hangzhou Global Scientific and Technological Innovation Center, Hangzhou, China

Correspondence

Lifeng Yang and Huabin Xing, Key Laboratory of Biomass Chemical Engineering of Ministry of Education, College of Chemical and Biological Engineering, Zhejiang University, Hangzhou 310027, China.
Email: lifeng_yang@zju.edu.cn and xinghb@zju.edu.cn

Funding information

National Natural Science Foundation of China, Grant/Award Numbers: 22122811, 22108240, 22278354

Abstract

Multiple impurities removal represents one of the most daunting challenges in gas purification, but the attainment of efficient adsorptive separation is hindered by the difficulty in designing adsorbents that could simultaneously capture different impurities. Herein, we revealed a molecular trap within Zn-trz-ox (trz = 1,2,4-triazole; ox = oxalic acid) that featured positive H and negative O sites, and the suitable pore size, which exhibited remarkable one-step C₂H₄ purification performance directly from quaternary C₂H₄/C₂H₂/C₂H₆/CO₂ mixtures. The separation selectivities of C₂H₄ with respect to CO₂, C₂H₂, and C₂H₆ are 9.8, 2.6, and 2.5, higher than the sole adsorbent yet reported. Meanwhile, polymer grade C₂H₄ (≥99.95%) could be directly obtained with record C₂H₄ productivity of 1.5 mol kg⁻¹, over 10 times higher than that of the previous benchmark material. The deep insight into the binding behavior revealed by simulation studies offers important clues for the design of advanced adsorbent for multiple impurities capture.

KEYWORDS

ethylene purification, gas separation, metal-organic frameworks, multiple impurities, one-step

1 | INTRODUCTION

Ethylene (C₂H₄) is one of the largest basic chemicals and its production¹ is expected to exceed 220 million tons in 2023. However, due to complex impurities that exist in C₂H₄ from cracking gas^{2,3} (e.g., ~9% C₂H₆, ~1% C₂H₂, ~1% CO₂), C₂H₄ purification currently is implemented by cascade procedures that consist of catalytic hydrogenation, absorption using caustic soda and cryogenic distillation.⁴ The cumbersome and energy-intensive nature of the process creates the necessity to develop an energy-efficient purification process.

The significant advance in porous materials⁵⁻¹⁷ in the last decade has aroused interests of researchers to seek adsorptive separations to make the challenging separation processes more energy-efficient. The

developed ordered-assembly porous materials, like metal-organic frameworks (MOFs),¹⁸⁻²⁴ covalent organic frameworks (COFs),^{25,26} etc, provide an excellent platform for tailor-made porous materials that are adaptive for different guest molecules and have obtained considerable achievements in C₂H₄ purification. Porous materials decorated with ordered anions,³ and polar functional groups,²⁷ like -OH, open metal sites,²⁸ have realized highly efficient capture of trace C₂H₂ from C₂H₄. As the above mixtures are mixed with C₂H₆, the difficulty of C₂H₄ purification is apparently increased, which is not only due to the more complex components but also the distinctly different properties between C₂H₂ and C₂H₆. The introduction of aromatic-based rings (e.g., heterocyclic rings, benzene rings, porphyrin rings) to provide C-H binding sites within confined space is the common strategy to afford higher C₂H₂, C₂H₆ affinity than C₂H₄, certainly, the

confined space with suitable pore size and shape is the prerequisite. Except for the inert surface, the accessible N, and F sites as well as the uncoordinated O atoms are also utilized to enhance C_2H_2 , C_2H_6 adsorption, and Zn-ad-int,²⁹ $CuTiF_6$ -TPPY,³⁰ and PCP-FDCA³¹ have exhibited attractive separation performance. It is rationally speculated that the co-existence of CO_2 would cause the separation process to be more complex, and Chen et al.³² reported the case to obtain high-purity C_2H_4 from mixtures with CO_2 , but the process was based on the cascade utilization of three porous materials. Until 2021, the first example of Zn-atz-oba³³ was reported that realized one-step C_2H_4 purification, however, the low separation selectivity resulted in its unsatisfied separation performance. Overall, the one-step C_2H_4 purification from the quaternary mixtures still remains a daunting challenge.

As revealed by the distribution of surface electrostatic potential of molecules as well as the molecular sizes, the obvious properties difference could be observed between CO_2 , C_2H_2 , and C_2H_6 , as well as the close properties between C_2H_6 and C_2H_4 (Figure 1A; Figure S1). In detail, C_2H_2 and CO_2 had similar molecular sizes (~ 3.3 Å), but exhibited opposite surface electrostatic potential distribution, which made the simultaneous removal of CO_2 and C_2H_2 difficult. Meanwhile, the selective capture of C_2H_6 from C_2H_4 remains challenging,^{34–37} and in general, a trap with matched pore size to

C_2H_6 and high-density weak van der Waals or electronegative binding sites was designed to realize the favorable adsorption toward C_2H_6 than C_2H_4 . However, due to the weak affinity, such a tailor-made trap was always not beneficial to the deep removal of trace C_2H_2 and CO_2 with small molecular sizes.^{38–41} The widely distributed kinetic sizes (3.3–4.4 Å) as well as their differential polarity required different binding space to afford enough affinity with multiple molecules (Table S1).

Herein, we revealed a molecular trap within a zinc MOF (Zn-trz-ox) with a suitable cage size as well as the binding environment that showed benchmark one-step C_2H_4 purification performance from $C_2H_4/C_2H_2/C_2H_6/CO_2$ quaternary mixtures. Benefiting from the assembly nature of multiple ligands, the trap was simultaneously embedded with high-density negative O sites (from pillar ligands) and positive H sites (from layer ligands), and the multiple binding space (3.9–5.1 Å) enabled the effective trap of C_2H_6 , C_2H_2 , CO_2 molecules simultaneously. The calculated ideal adsorption solution theory (IAST) selectivities of CO_2/C_2H_4 , C_2H_2/C_2H_4 , and C_2H_6/C_2H_4 mixtures were 9.8, 2.6, and 2.5, respectively, significantly surpassing the previous benchmark materials (1.6, 1.8, and 1.3). Polymer grade C_2H_4 ($>99.95\%$) could be directly obtained from $C_2H_4/C_2H_2/C_2H_6/CO_2$ quaternary mixtures with record C_2H_4 productivity of 1.5 mol kg^{-1} . The simulation studies further provided a molecular-level understanding of the separation mechanism.

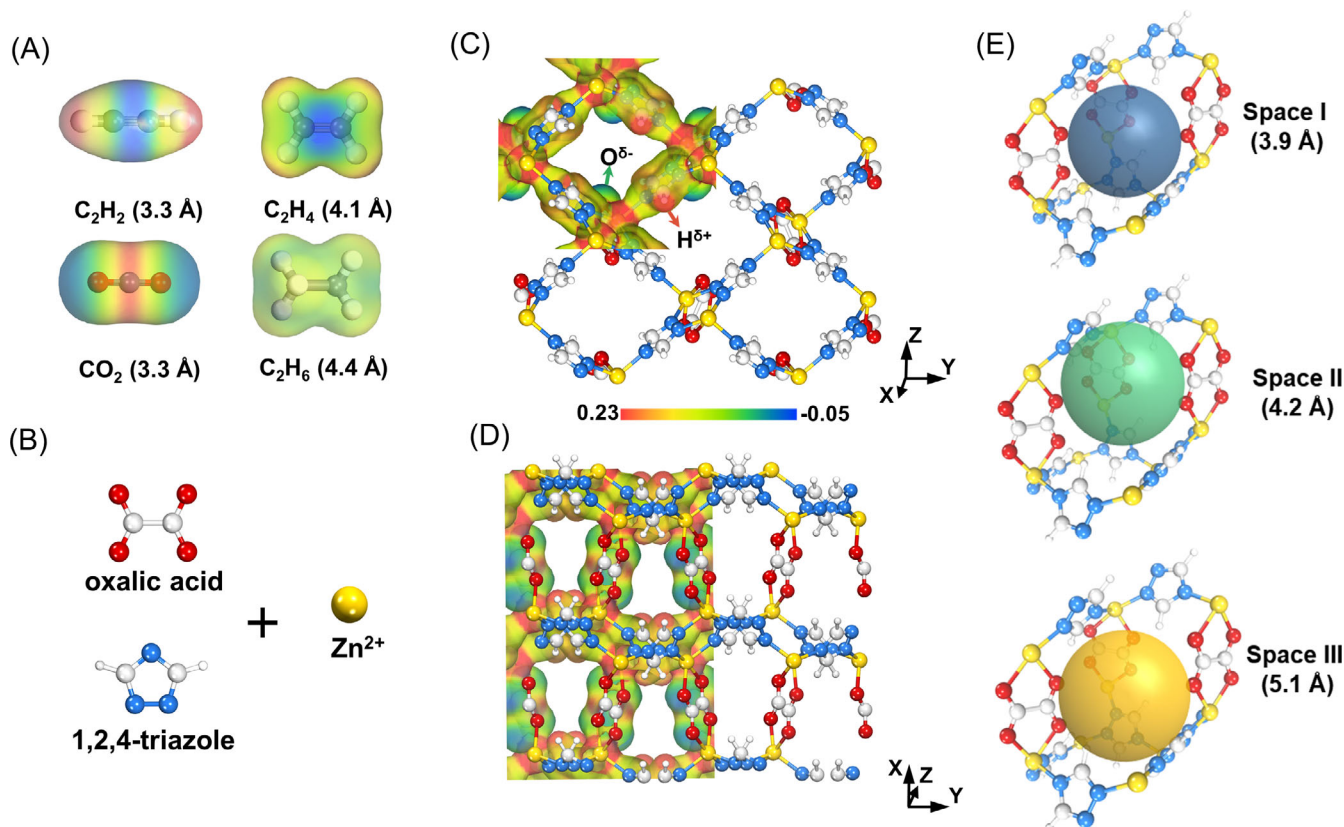


FIGURE 1 The gases properties, and pore structure of Zn-trz-ox. (A) Molecular dynamics size and the surface electrostatic potential of C_2H_4 , C_2H_2 , C_2H_6 , and CO_2 . (B) Zn-trz-ox is based upon the assembly of oxalic acid ligands, 1,2,4-triazole ligands, and Zn^{2+} ions. (Framework: Zn, gold; O, dark red; N, light blue; C, gray-25%; H, gray-5%.) Views of the electrostatic potential and the pore structure of Zn-trz-ox when viewed along the (C) x-axis and (D) z-axis, respectively. (E) Mapping of the multiple binding space within Zn-trz-ox.

2 | EXPERIMENTAL

2.1 | Materials

All chemicals were commercially available and used as purchased without further purification.

2.2 | Synthesis of Zn-trz-ox

Zn-trz-ox was prepared according to the reported method⁴² with some modifications. A mixture of $\text{ZnC}_2\text{O}_4 \cdot 2\text{H}_2\text{O}$ (7 mmol, 1.33 g), 1,2,4-triazole (Htrz) (30 mmol, 2.07 g), MeOH (60 mL) was sealed in a 100 mL Teflon-lined autoclave and stirred under room temperature for half an hour. Then the solution was sonicated for 5 min. The autoclave was sealed and placed in a homogeneous reactor with a rotation rate of 45 rpm, kept at 180°C for 2 days, then naturally cooled to room temperature. The as-synthesized sample Zn-trz-ox was washed with fresh MeOH and H_2O , and then activated at 373 K in a vacuum for 12 h (Figure S2).

2.3 | Adsorption isotherms measurement

Single component adsorption isotherms of C_2H_4 , C_2H_2 , C_2H_6 , and CO_2 (273, 298, and 313 K) were measured on ASAP 2460 (Micromeritics, USA) instruments. Before each measurement, approximately 100 mg of Zn-trz-ox material was loaded into a quartz analysis tube and heated at 373 K for 8 h under a dynamic pressure below 35 mTorr. Subsequently, the activated sample was purged with N_2 and then transferred to the analysis port.

2.4 | Breakthrough experiment and simulations

The breakthrough experiments were conducted on self-assembled dynamic gas breakthrough equipment. In a typical procedure, a stainless-steel column (Φ 4.6 × 150 mm) packed with 1.03 g of Zn-trz-ox material was activated by purging with N_2 (10 mL min^{-1}) at 373 K for 12 h. A $\text{CO}_2/\text{C}_2\text{H}_2/\text{C}_2\text{H}_6/\text{C}_2\text{H}_4/\text{He}$ (0.7/1.5/9.1/76.3/12.4, v/v/v/v/v) mixture was introduced to the column with a gas flow rate of 1.8 mL min^{-1} and $\text{C}_2\text{H}_2/\text{C}_2\text{H}_6/\text{C}_2\text{H}_4$ (1.2/9.3/89.5, v/v/v) mixture at a rate of 1.7 mL min^{-1} under 273 K. The concentration of the gas eluted from the outlet was detected by chromatography (GC-490, Agilent) with a thermal conductivity detector. After the breakthrough experiment, the sample was regenerated with N_2 at 373 K for 4 h at a flow rate of 5 mL min^{-1} . The corresponding breakthrough simulations were also undertaken using the methodology described in the literature⁴³; further details are provided in the [Supplementary Materials](#).

2.5 | Computational details

Dispersion-corrected density functional theory (DFT-D) calculations were performed with the CASTEP module implemented in Materials

Studio version 2017R2. A semi-empirical addition (the Grimme method) of dispersive forces to conventional DFT was included in the calculation to account for van der Waals interactions. Calculations were performed under the generalized gradient approximation (GGA) with Perdew–Burke–Ernzerhof (PBE) exchange–correlation. Cut-off energy of 534 eV and a $3 \times 2 \times 2$ *k*-point mesh were found to be enough for the total energy to converge within $5 \times 10^{-6} \text{ eV atom}^{-1}$. We first optimized the structure of Zn-trz-ox, which agreed well with the reported Zn-trz-ox (guest-free) structure. $\text{CO}_2/\text{C}_2\text{H}_2/\text{C}_2\text{H}_6/\text{C}_2\text{H}_4$ gas molecules were then introduced to various locations of the pore channel, followed by a full structural relaxation. The static binding energy (at $T = 0 \text{ K}$) was then calculated: $\text{EB} = \text{E}(\text{MOF}) + \text{E}(\text{gas}) - \text{E}(\text{MOF} + \text{gas})$.

The molecular electrostatic potential-based (ESP) charges were calculated using the DMol3 modules in Materials Studio with GGA with PBE exchange–correlation. The Grand Canonical Monte Carlo (GCMC) simulations were performed using the Sorption module in Material Studio version 2017R2. The non-bonded interactions between atoms were calculated using the Lennard–Jones (LJ 6–12) potential. The atoms of the framework and gas molecules were calculated using the Universal Force Field. The beneficial adsorption sites were simulated by the locate task and Metropolis method. The cutoff radius was set to be 12 Å and the Ewald summation method was used to calculate the electrostatic interactions between the guest molecules and the MOFs. A crystallographic cell of $3 \times 2 \times 2$ was used during the GCMC simulation. For each state point, the system was equilibrated for 5×10^6 Monte Carlo steps before collecting the final data for 5×10^6 Monte Carlo steps.

3 | RESULTS AND DISCUSSION

3.1 | Pore structure and $\text{CO}_2/\text{C}_2\text{H}_2/\text{C}_2\text{H}_6/\text{C}_2\text{H}_4$ adsorption property

Zn-trz-ox (trz = 1,2,4-triazole, ox = oxalate) exhibits a well-proportioned three-dimensional (3D) pore cage ($5.85 \times 4.62 \text{ Å}$; Figures S3 and S4), constructed by stacking layers of zinc(II) ions interconnected by 1,2,4-triazole ligands and pillars of oxalate ions ligands (Figure 1B). Through the electrostatic potential map of the framework (Figure 1C,D), we could clearly observe the co-existence of negative O sites from oxalate and the positive H sites from triazole, and the good distribution of binding sites within the suitable confined space provides several potential binding space (Figure 1E), which is well matched to the size range of series C2 and CO_2 molecules. Its permanent porosity is verified by N_2 adsorption isotherm at 77 K with the Brunauer–Emmett–Teller surface area of $561 \text{ m}^2 \text{ g}^{-1}$ and the pore size of about 0.5 nm (Figure S5). It is speculated that Zn-trz-ox with suitable channel space and a judicious combination of positive and negative sites is potential in complex impurities capture.

We collected the single-component adsorption and desorption isotherms of C_2H_4 , C_2H_2 , C_2H_6 , and CO_2 at 273, 298, and 313 K (Figure 2A; Figures S6–S8; Table S2). The measured capacities of

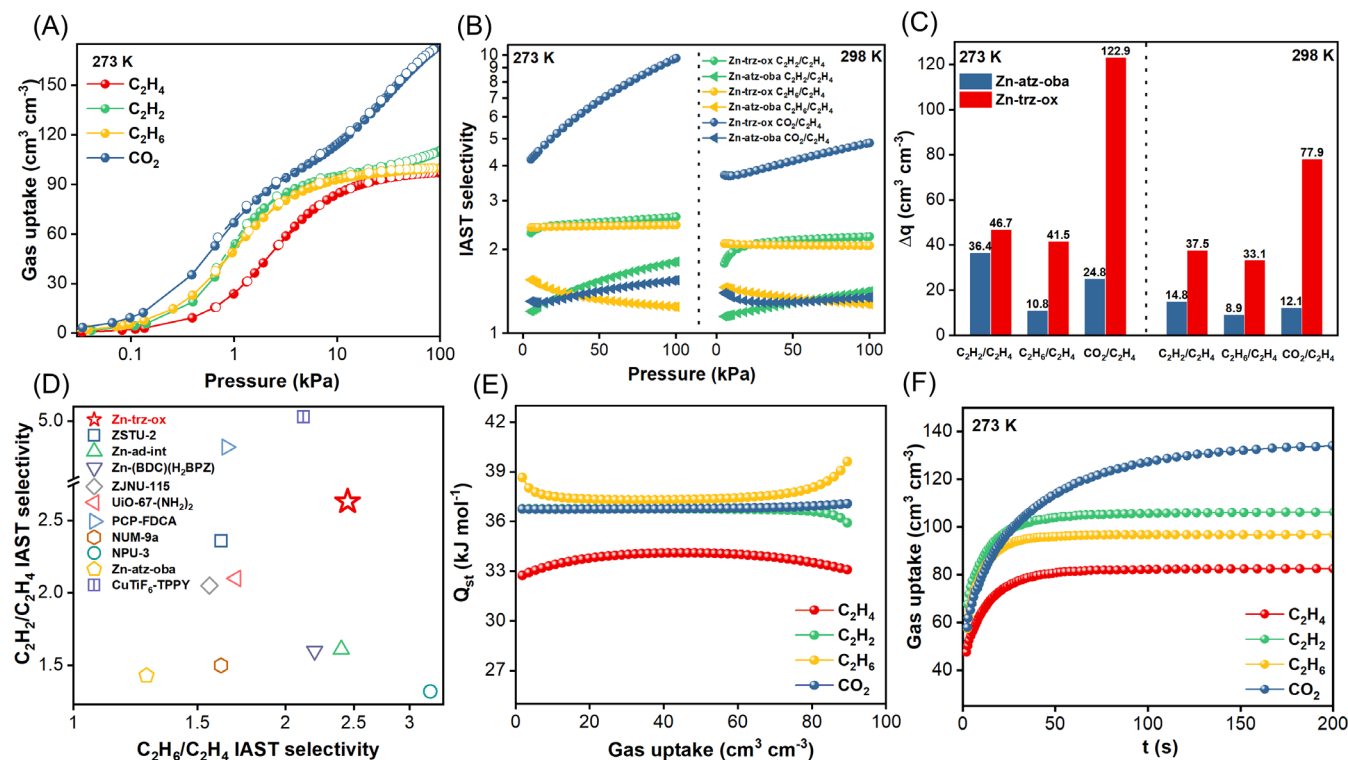


FIGURE 2 The separation performance of Zn-trz-ox. (A) Adsorption and desorption isotherms of C_2H_4 , C_2H_2 , C_2H_6 , CO_2 on Zn-trz-ox at 273 K. (B) A comparison for C_2H_2/C_2H_4 , C_2H_6/C_2H_4 , and CO_2/C_2H_4 (50/50, v/v) selectivities among Zn-atz-oba and Zn-trz-ox at 273 K and 298 K. (C) The separation potential for CO_2/C_2H_4 , C_2H_2/C_2H_4 , and C_2H_6/C_2H_4 (50/50, v/v) mixture with Zn-atz-oba and Zn-trz-ox at 273 K and 298 K. (D) A comparison for the C_2H_6/C_2H_4 and C_2H_2/C_2H_4 selectivities among representative porous materials. (E) The isosteric heat of adsorption, Q_{st} , for C_2H_4 , C_2H_2 , C_2H_6 , and CO_2 on Zn-trz-ox. (F) Time-dependent gas uptake profiles of C_2H_4 , C_2H_2 , C_2H_6 , and CO_2 at 40 kPa and 273 K.

C_2H_2 , C_2H_6 , and CO_2 exceeded C_2H_4 throughout the whole pressure (0–100 kPa) and wide temperature range (273–313 K), and the obviously steeper adsorption curve indicated the preferential binding affinity of C_2H_2 , C_2H_6 , and CO_2 than C_2H_4 . Specifically, the uptakes of CO_2 and C_2H_2 reached 66.9 and 52.8 $cm^3 cm^{-3}$ at 1 kPa, respectively, and the value of C_2H_6 was up to 92.2 $cm^3 cm^{-3}$ at 9 kPa, enabling the remarkable trace gas capture ability of the material. To intuitively assess the separation ability of Zn-trz-ox toward the mixtures, the IAST was employed (Figure 2B; Figure S9). The calculated IAST selectivities of Zn-trz-ox for CO_2/C_2H_4 , C_2H_2/C_2H_4 , and C_2H_6/C_2H_4 mixtures (50/50) reached 9.8, 2.6, and 2.5, respectively, higher than the previous benchmark material Zn-atz-oba³³ (1.6, 1.8, and 1.3) at 273 K and 100 kPa (Table S3). Around ambient temperatures, Zn-trz-ox still exhibited high separation selectivities, around 4.9 for CO_2/C_2H_4 , 2.2 for C_2H_2/C_2H_4 , and 2.1 for C_2H_6/C_2H_4 at 298 K. The separation potential ($\Delta q = q_1 y_2 / y_1 - q_2$) that represents the combined selectivity-capacity metric was also calculated (Figure 2C; Figure S10), and the high value for all CO_2/C_2H_4 (273 K: 122.9 $cm^3 cm^{-3}$, 298 K: 77.9 $cm^3 cm^{-3}$), C_2H_2/C_2H_4 (273 K: 46.7 $cm^3 cm^{-3}$, 298 K: 37.5 $cm^3 cm^{-3}$), C_2H_6/C_2H_4 (273 K: 41.5 $cm^3 cm^{-3}$, 298 K: 33.1 $cm^3 cm^{-3}$) components under 273 and 298 K rendered Zn-trz-ox to be a promising adsorbent for C_2H_4 purification (Table S4). Moreover, we also evaluated the separation performance of Zn-trz-ox for $C_2H_2/C_2H_4/C_2H_6$ mixtures, the balanced C_2H_6/C_2H_4 and C_2H_2/C_2H_4

separation selectivities were higher than the most reported materials^{29–31,33,37,44–46} (Figure 2D), such as Zn-ad-int (2.4, 1.6),²⁹ UiO-67-(NH_2)₂ (1.7, 2.1).⁴⁵ The heat of adsorption (Q_{st}), calculated by implementing the Clausius–Clapeyron equation, was based on the isotherms of adsorption at 273, 298, and 313 K for different gases. The Q_{st} values of C_2H_2 (36.8), C_2H_6 (38.7), and CO_2 (36.7) were higher than that of C_2H_4 (32.7), demonstrating the weak C_2H_4 binding affinity of Zn-trz-ox (Figure 2E). In addition, we also measured the time-dependent adsorption profiles, and though the different molecular sizes, C_2H_4 , C_2H_2 , C_2H_6 , and CO_2 show quick adsorption kinetics with the calculated diffusion time constants (D_e/r_c^2) of 0.032, 0.036, 0.036, and 0.016 s^{-1} , respectively at 273 K (Figure 2F; Figure S11). The calculated competing adsorption isotherms of Zn-trz-ox for $CO_2/C_2H_2/C_2H_6/C_2H_4$ (1/1/1/1, v/v/v/v) mixture also showed that the uptakes of Zn-trz-ox for C_2H_2 , C_2H_6 , and CO_2 were much higher than that of C_2H_4 (Figure S12).

3.2 | Computational simulation studies

To gain deep insight into the interactions between the guest molecules and the framework, DFT-D calculations were performed to determine the adsorption configuration and binding energies of C_2H_2 , C_2H_6 , CO_2 , and C_2H_4 . It was observed that the O atoms of the adsorbed CO_2 molecule formed two hydrogen bonds with H atoms

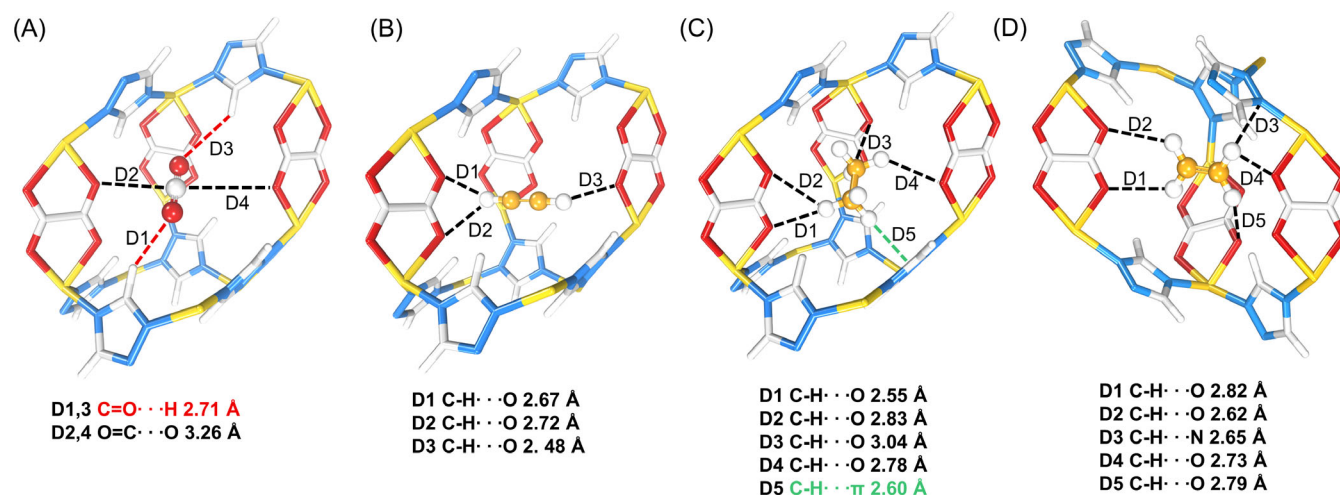


FIGURE 3 The First-principles dispersion-corrected density functional theory calculations for Zn-trz-ox. Calculated binding sites of (A) CO₂, (B) C₂H₂, (C) C₂H₆, and (D) C₂H₄ on Zn-trz-ox; The closest contacts between framework atoms and the gas molecules are defined by the distances (in Å), and the distances include the van der Waals radius of atoms. (Framework: Zn, gold; O, dark red; N, light blue; C, gray-25%; H, gray-5%.)

from the two triazoles (H...O = 2.71 Å) (Figure 3A), and the C atom of CO₂ was also bonded with O from the oxalate ring (O=C...O, 3.26 Å). The multiple interactions enhanced the affinity between CO₂ and the framework for trace CO₂ capture. For C₂H₂ (Figure 3B), the characteristic linear molecular shape of C₂H₂ allowed close access to the narrow corners of the pore cage. C₂H₂ formed three C-H...O hydrogen bonds with three O atoms of two oxalic acids with short H...O distances (2.48, 2.67, and 2.72 Å, respectively). The adsorbed C₂H₆ molecules were observed to form multiple hydrogen bonding interactions and C-H...C electrostatic interactions mainly with three oxalic acid rings (Figure 3C). Moreover, the H atoms of C₂H₆ was in close contact with many atoms from these rings, forming four hydrogen bonds with O atoms from three oxalic acids (H...O = 2.55 Å, H...O = 2.83 Å, H...O = 3.04 Å, H...O = 2.78 Å, respectively). It also formed C-H...π van der Waals (vdW) interactions with one triazole ring (C-H...π = 2.60 Å). The phenomenon indicated a high binding force between C₂H₆ and the main framework. The adsorbed C₂H₄ formed four relatively weak C-H...O hydrogen bonds (H...O = 2.62, 2.73, 2.79, and 2.82 Å) and one C-H...N hydrogen bond (H...N = 2.65 Å) by interacting with O atoms of oxalic acid and an N atom of triazole (Figure 3D). The Grand Canonical Monte Carlo (GCMC) simulations are used to reveal the density distribution of C₂H₄, C₂H₂, C₂H₆, and CO₂ within Zn-trz-ox, and the order of CO₂ > C₂H₂ > C₂H₆ > C₂H₄ is consistent with their sequence of adsorption capacities at 100 kPa and 298 K (Figure S13). CO₂ molecules were evenly distributed across the entire Zn-trz-ox framework, while C₂H₆ molecules predominantly adhered to the center of the oxalate ionic pillars. For C₂H₂ molecules, their primary adsorption sites were within the center of the oxalate ionic pillars and at the junction of the azole and oxalate ionic pillars, while C₂H₄ molecules were loosely dispersed within the central region of Zn-trz-ox framework. The interaction of the ethylene molecule with the surrounding framework was weak because its planar shape was less compatible with that framework structure. The calculated

binding energies of C₂H₂, C₂H₆, and CO₂ were 42.6, 43.6, and 40.7 kJ mol⁻¹, respectively (Table S5). These values were higher than that of C₂H₄ (33.6 kJ mol⁻¹). This observation is consistent with the trend of experimental Qst. However, since DFT-D calculated binding energies are determined at 0 K, its value is slightly higher than that of Qst. Understanding the adsorption behavior of gases with different properties was instructive for porous materials design.

3.3 | Breakthrough experiments and cycling tests

To evaluate the separation ability of Zn-trz-ox toward mixtures, we firstly performed the simulated transient breakthrough curves of Zn-trz-ox, Zn-atz-oba for CO₂/C₂H₂/C₂H₆/C₂H₄/He (0.7/1.5/9.1/76.3/12.4, v/v/v/v/v) mixtures at 273 K, and preferential adsorption behavior of CO₂/C₂H₂/C₂H₆ than C₂H₄ is clearly observed, indicating its potential separation ability (Figure 4A; Figures S14 and S15). Furthermore, we also conducted the dynamic breakthrough performance for the above-mentioned multiple mixtures at a flow rate of 1.8 mL min⁻¹ at 273, 298, and 313 K (Figure 4B; Figure S16). C₂H₄ was firstly eluted at 42.1 min, and after an interval of approximately 30 min, the residual components of C₂H₂, C₂H₆, and CO₂ were subsequently observed, demonstrating the superior capture ability of Zn-trz-ox toward the above impurities. It is noted that the different CO₂ capture performance in simulated and experimental breakthrough curves was attributed to its really low content as well as the difficulty in the accurate calculation of CO₂ working capacity (Table S6). As revealed by gas chromatography, C₂H₄ with purity greater than 99.95% could be directly obtained via single adsorption (Figure S17), and the C₂H₄ recovery was up to 33.6% at 298 K (Figure 4C; Table S7). The recovery was improved to 39.0% when decreasing the temperature to 273 K. It was noted that the C₂H₄ productivity of Zn-trz-ox was up to 1.5 mol kg⁻¹, which was almost over 10 times higher

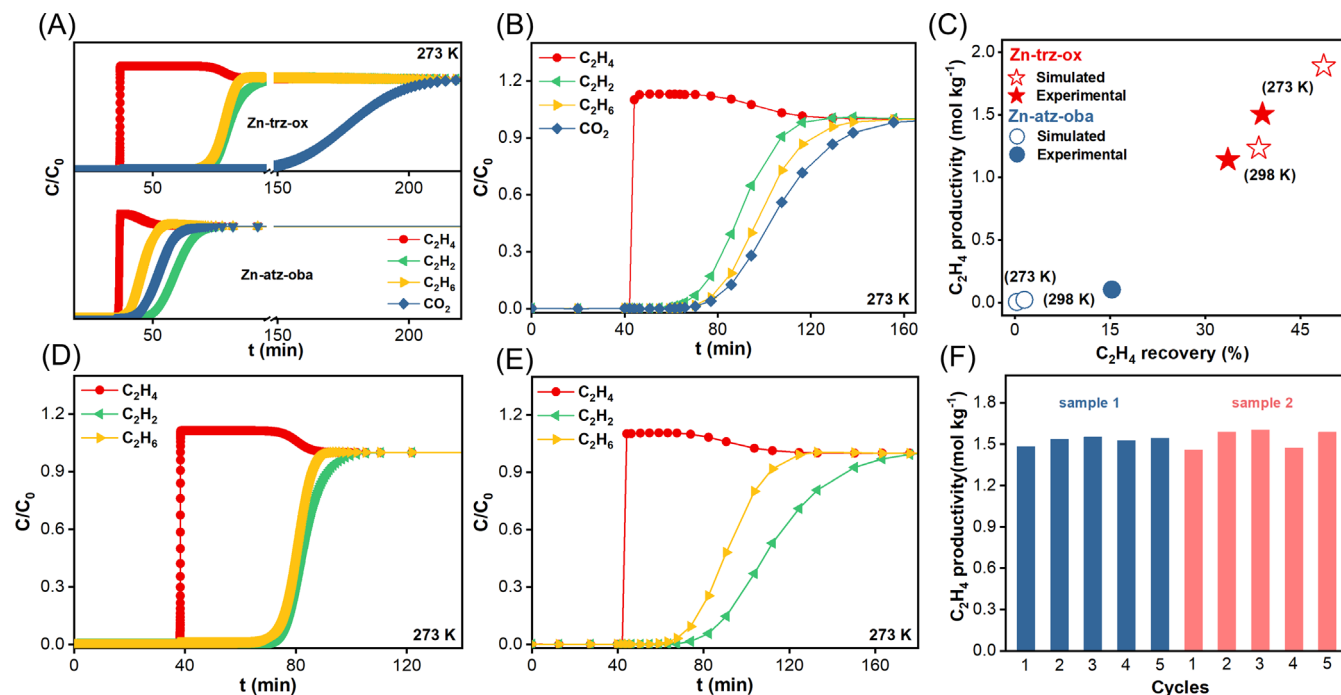


FIGURE 4 Simulated transient breakthrough curves, experimental dynamic breakthrough curves, and cycling tests. (A) The simulated transient breakthrough curves of Zn-atz-oba and Zn-trz-ox and (B) experimental dynamic breakthrough curves of Zn-trz-ox for CO₂/C₂H₂/C₂H₆/C₂H₄/He (0.7/1.5/9.1/76.3/12.4, v/v/v/v/v) mixture with a gas flow rate of 1.8 mL min⁻¹ at 273 K. (C) Comparison of the captured C₂H₄ recovery and C₂H₄ productivity from simulated and experimental breakthrough experiments of CO₂/C₂H₂/C₂H₆/C₂H₄/He (0.7/1.5/9.1/76.3/12.4, v/v/v/v/v) using Zn-atz-oba and Zn-trz-ox. It is noted that the experimental recovery and productivity value of Zn-atz-oba is derived from the reported data of CO₂/C₂H₂/C₂H₆/C₂H₄ (1/1/1/1, v/v/v/v). (D) The simulated transient breakthrough curves and (E) experimental dynamic breakthrough curves of Zn-trz-ox for C₂H₂/C₂H₄/C₂H₆/C₂H₄ (1.2/9.3/89.5, v/v/v) mixture with a flow rate of 1.7 mL min⁻¹ at 273 K. (F) Five continuous breakthrough cycles of two different samples at a flow rate of 1.8 mL min⁻¹ on Zn-trz-ox at 273 K. (The sample was regenerated with N₂ at 373 K for 4 h at a flow rate of 5 mL min⁻¹.)

than the previous benchmark material (0.1 mol kg⁻¹ for Zn-atz-oba), as indicated by both simulated and experimental results. Note that the recovery and productivity of Zn-atz-oba were calculated from a breakthrough experiment for C₂H₂/C₂H₄/C₂H₆/CO₂ (1:1:1:1) mixture.³³ In addition, the ternary mixture separation performance of Zn-trz-ox was also evaluated (Table S8). The simulated transient breakthrough curve with the three mixtures suggested that high-purity C₂H₄ can be separated from the C₂H₂/C₂H₄/C₂H₆ ternary mixture with Zn-trz-ox in one-step way (Figure 4D). The practical separation ability of Zn-trz-ox was further validated again by dynamic breakthrough experiments (Figure 4E). The elution time for C₂H₂ and C₂H₆ (74.0 and 67.6 min) was also significantly later than for C₂H₄ (42.1 min) at a flow rate of 1.7 mL min⁻¹ at 273 K, and 99.95% purity C₂H₄ could be obtained with the C₂H₄ productivity of 1.742 mol kg⁻¹. The stability of adsorbents was essentially vital to their practical use, and we found that the crystalline structure of Zn-trz-ox was well maintained after exposure to air for 1 year, acid treatment for 1 month, or cycling breakthrough experiments (Figure S18). The C₂H₂ uptakes of the samples after acid treatment and cycling breakthrough experiments were close to that of the pristine material (Figure S19). Meanwhile, Zn-trz-ox was thermally stable until the temperature of 350°C (Figure S20). During the five consecutive breakthrough cycles, the separation performance of

Zn-trz-ox from different batches was well kept (Figure 4F). To demonstrate the repeatability of C₂H₄ purification performance, another batch of Zn-trz-ox was synthesized and it showed almost invariable uptake, as well as the separation selectivity. (Table S3; Figures S8 and S9, as well as Figure 4F).

4 | CONCLUSIONS

In summary, we discovered a highly efficient molecular trap within the zinc MOF, Zn-trz-ox. Based on the optimal cage size and multiple binding environments, Zn-trz-ox demonstrated exceptional one-step C₂H₄ purification performance from complex C₂H₄/C₂H₂/C₂H₆/CO₂ quaternary mixtures along with the record CO₂/C₂H₄, C₂H₂/C₂H₄, and C₂H₆/C₂H₄ separation selectivity. 99.95% purity C₂H₄ could be directly obtained with a high C₂H₄ productivity. The remarkable separation performance demonstrates the advance of the strategy for different kinds of impurities captures based on the multiple binding space, which could be constructed by leveraging the distinct functional groups carried by different ligands via reticular chemistry. The study also deepens our understanding of the pore structure and microenvironmental regulation of porous materials in dealing with the separation of complex gas mixtures.

AUTHOR CONTRIBUTIONS

Tangyin Wu: Data curation (lead); formal analysis (lead); investigation (lead); validation (lead); writing – original draft (lead). **Cong Yu:** Formal analysis (supporting); investigation (supporting); methodology (supporting). **Rajamani Krishna:** Software (lead); writing – review and editing (supporting). **Zhensong Qiu:** Data curation (supporting); validation (supporting). **Hanqian Pan:** Data curation (supporting); formal analysis (supporting); methodology (supporting); validation (supporting). **Peixin Zhang:** Formal analysis (supporting); investigation (supporting); methodology (supporting). **Xian Suo:** Project administration (supporting); supervision (supporting); validation (supporting). **Lifeng Yang:** Conceptualization (equal); funding acquisition (equal); supervision (equal); writing – review and editing (lead). **Xili Cui:** Funding acquisition (equal); project administration (equal); writing – review and editing (supporting). **Huabin Xing:** Conceptualization (equal); funding acquisition (equal); project administration (lead); supervision (equal).

ACKNOWLEDGMENTS

This work was supported by the National Natural Science Foundation of China (Nos. 22122811, 22108240, and 22278354).

DATA AVAILABILITY STATEMENT

The numerical data from Figures 2 and 4, and Figures S5, S7, S9–S11, S14–S16, S19 are tabulated in the raw_data1.xlsx and raw_data2.xlsx of Supplementary Material. In addition, the input information from the calculation settings is included in the Computational details and Supplementary Materials. The data that support the findings of this study are available from the corresponding author upon reasonable request.

ORCID

Rajamani Krishna  <https://orcid.org/0000-0002-4784-8530>

Lifeng Yang  <https://orcid.org/0000-0002-2810-3023>

Xili Cui  <https://orcid.org/0000-0002-5600-8402>

Huabin Xing  <https://orcid.org/0000-0002-7418-0046>

REFERENCES

1. Konzept Analytics. Global Ethylene Market (By Production Capacity & Demand): Insights & Forecast with Potential Impact of COVID-19 (2023-2027). Publication 5531033, Research And Markets, 2023; www.researchandmarkets.com/r/o4wnhy
2. Liao PQ, Zhang WX, Zhang JP, Chen XM. Efficient purification of ethene by an ethane-trapping metal-organic framework. *Nat Commun*. 2015;6(1):8697.
3. Cui X, Chen K, Xing H, et al. Pore chemistry and size control in hybrid porous materials for acetylene capture from ethylene. *Science*. 2016; 353(6295):141-144.
4. Ren T, Patel M, Blok K. Olefins from conventional and heavy feedstocks: energy use in steam cracking and alternative processes. *Energy*. 2006;31(4):425-451.
5. Cai X, Sholl DS. Point defects control guest molecule diffusion in the 1D pores of Zn(tbip). *J Phys Chem C*. 2022;126(33):14321-14328.
6. Li J-R, Sculley J, Zhou H-C. Metal-organic frameworks for separations. *Chem Rev*. 2012;112(2):869-932.
7. Ding M, Flaig RW, Jiang HL, Yaghi OM. Carbon capture and conversion using metal-organic frameworks and MOF-based materials. *Chem Soc Rev*. 2019;48(10):2783-2828.
8. Zhou H-C, Kitagawa S. Metal-organic frameworks (MOFs). *Chem Soc Rev*. 2014;43(16):5415-5418.
9. Liao PQ, Huang NY, Zhang WX, Zhang JP, Chen XM. Controlling guest conformation for efficient purification of butadiene. *Science*. 2017;356(6343):1193-1196.
10. Zeng H, Xie M, Wang T, et al. Orthogonal-array dynamic molecular sieving of propylene/propane mixtures. *Nature*. 2021;595(7868):542-548.
11. Ye Y, Xie Y, Shi Y, et al. A microporous metal-organic framework with unique aromatic pore surfaces for high performance C₂H₆/C₂H₄ separation. *Angew Chem Int Ed*. 2023;62(21):e202302564.
12. Liu Y, Chen L, Yang L, et al. Porous framework materials for energy & environment relevant applications: a systematic review. *Green Energy Environ*. 2023. doi:10.1016/j.gee.2022.12.010
13. Ma X, Kumar P, Mittal N, et al. Zeolitic imidazolate framework membranes made by ligand-induced permselectivation. *Science*. 2018; 361(6406):1008-1011.
14. Dinakar B, Forse AC, Jiang HZH, et al. Overcoming metastable CO₂ adsorption in a bulky diamine-appended metal-organic framework. *J Am Chem Soc*. 2021;143(37):15258-15270.
15. Zhou S, Shekhah O, Jin T, et al. A CO₂-recognition metal-organic framework membrane for continuous carbon capture. *Chem*. 2023; 9(5):1182-1194.
16. Huang J, Peng J, Wei X, Du S, Yang C, Xiao J. Synergetic thermodynamic/kinetic separation of C₃H₈/CH₃F on carbon adsorbents for ultrapure fluoromethane electronic gas. *AIChE J*. 2023; 69(5):e18027.
17. Chai Y, Han X, Li W, et al. Control of zeolite pore interior for chemoselective alkyne/olefin separations. *Science*. 2020;368(6494):1002-1006.
18. Zhang Z, Peh SB, Wang Y, Kang C, Fan W, Zhao D. Efficient trapping of trace acetylene from ethylene in an ultramicroporous metal-organic framework: synergistic effect of high-density open metal and electronegative sites. *Angew Chem Int Ed*. 2020;59(43):18927-18932.
19. Yu C, Guo Z, Yang L, et al. A robust metal-organic framework with scalable synthesis and optimal adsorption and desorption for energy-efficient ethylene purification. *Angew Chem Int Ed*. 2023;62(16): e202218027.
20. Ding Q, Zhang Z, Yu C, et al. Exploiting equilibrium-kinetic synergetic effect for separation of ethylene and ethane in a microporous metal-organic framework. *Sci Adv*. 2020;6(15):eaaz4322.
21. Wang JW, Fan SC, Li HP, Bu X, Xue YY, Zhai QG. De-linker-enabled exceptional volumetric acetylene storage capacity and benchmark C₂H₂/C₂H₄ and C₂H₂/CO₂ separations in metal-organic frameworks. *Angew Chem Int Ed*. 2023;62(10):e202217839.
22. Macreadie LK, Idrees KB, Smoljan CS, Farha OK. Expanding linker dimensionality in metal-organic frameworks for sub-Ångstrom pore control for separation applications. *Angew Chem Int Ed*. 2023;62(28): e202304094.
23. Su K, Wang W, Du S, Ji C, Yuan D. Efficient ethylene purification by a robust ethane-trapping porous organic cage. *Nat Commun*. 2021; 12(1):3703.
24. Wu H, Chen Y, Yuan Y, et al. The modulation of ethane-selective adsorption performance in series of bimetal PCN-250 metal-organic frameworks: impact of metal composition. *AIChE J*. 2022;68(1): e17385.
25. Jin F, Lin E, Wang T, et al. Bottom-up synthesis of 8-connected three-dimensional covalent organic frameworks for highly efficient ethylene/ethane separation. *J Am Chem Soc*. 2022;144(12):5643-5652.
26. He C, Wang Y, Chen Y, et al. Microregulation of pore channels in covalent-organic frameworks used for the selective and efficient separation of ethane. *ACS Appl Mater Interfaces*. 2020;12(47):52819-52825.
27. Li J, Jiang L, Chen S, et al. Metal-organic framework containing planar metal-binding sites: efficiently and cost-effectively

- enhancing the kinetic separation of C_2H_2/C_2H_4 . *J Am Chem Soc.* 2019;141(9):3807-3811.
28. Jiang C, Hao C, Wang X, et al. Constructing C_2H_2 anchoring traps within MOF interpenetration nets as C_2H_2/CO_2 and C_2H_2/C_2H_4 bifunctional separator. *Chem Eng J.* 2023;453:139713.
 29. Ding Q, Zhang Z, Liu Y, Chai K, Krishna R, Zhang S. One-step ethylene purification from ternary mixtures in a metal-organic framework with customized pore chemistry and shape. *Angew Chem Int Ed.* 2022; 61(35):e202208134.
 30. Zhang P, Zhong Y, Zhang Y, et al. Synergistic binding sites in a hybrid ultramicroporous material for one-step ethylene purification from ternary C_2 hydrocarbon mixtures. *Sci Adv.* 2022;8(23):eabn9231.
 31. Sun H, Chen F, Chen R, et al. Customizing metal-organic frameworks by lego-brick strategy for one-step purification of ethylene from a quaternary gas mixture. *Small.* 2023;19(21):2208182.
 32. Chen KJ, Madden DG, Mukherjee S, et al. Synergistic sorbent separation for one-step ethylene purification from a four-component mixture. *Science.* 2019;366(6462):241-246.
 33. Cao JW, Mukherjee S, Pham T, et al. One-step ethylene production from a four-component gas mixture by a single physisorbent. *Nat Commun.* 2021;12(1):6507.
 34. Wang Y, Hao C, Fan W, et al. One-step ethylene purification from an acetylene/ethylene/ethane ternary mixture by cyclopentadiene cobalt-functionalized metal-organic frameworks. *Angew Chem Int ed.* 2021;133(20):11451-11459.
 35. Di Z, Liu C, Pang J, et al. A metal-organic framework with nonpolar pore surfaces for the one-step acquisition of C_2H_4 from a C_2H_4 and C_2H_6 mixture. *Angew Chem Int Ed.* 2022;61(42):e202210343.
 36. Hao HG, Zhao YF, Chen DM, et al. Simultaneous trapping of C_2H_2 and C_2H_6 from a ternary mixture of $C_2H_2/C_2H_4/C_2H_6$ in a robust metal-organic framework for the purification of C_2H_4 . *Angew Chem Int Ed.* 2018;57(49):16067-16071.
 37. Wang GD, Li YZ, Shi WJ, Hou L, Wang YY, Zhu Z. One-step C_2H_4 purification from ternary $C_2H_6/C_2H_4/C_2H_2$ mixtures by a robust metal-organic framework with customized pore environment. *Angew Chem Int Ed.* 2022;61(28):e202205427.
 38. Jiang Y, Hu Y, Luan B, et al. Benchmark single-step ethylene purification from ternary mixtures by a customized fluorinated anion-embedded MOF. *Nat Commun.* 2023;14(1):401.
 39. Mukherjee S, Kumar N, Bezrukov AA, et al. Amino-functionalised hybrid ultramicroporous materials that enable single-step ethylene purification from a ternary mixture. *Angew Chem Int Ed.* 2021;60(19): 10902-10909.
 40. Dong Q, Zhang X, Liu S, et al. Tuning gate-opening of a flexible metal-organic framework for ternary gas sieving separation. *Angew Chem Int Ed.* 2020;59(50):22756-22762.
 41. Dong Q, Huang Y, Hyeon-Deuk K, et al. Shape- and size-dependent kinetic ethylene sieving from a ternary mixture by a trap-and-flow channel crystal. *Adv Funct Mater.* 2022;32(38):2203745.
 42. Lin JB, Nguyen TTT, Vaidhyanathan R, et al. A scalable metal-organic framework as a durable physisorbent for carbon dioxide capture. *Science.* 2021;374(6574):1464-1469.
 43. Krishna R. Metrics for evaluation and screening of metal-organic frameworks for applications in mixture separations. *ACS Omega.* 2020;5(28):16987-17004.
 44. Zhu B, Cao JW, Mukherjee S, et al. Pore engineering for one-step ethylene purification from a three-component hydrocarbon mixture. *J Am Chem Soc.* 2021;143(3):1485-1492.
 45. Gu XW, Wang JX, Wu E, et al. Immobilization of Lewis basic sites into a stable ethane-selective MOF enabling one-step separation of ethylene from a ternary mixture. *J Am Chem Soc.* 2022;144(6):2614-2623.
 46. Fan L, Zhou P, Wang X, Yue L, Li L, He Y. Rational construction and performance regulation of an In(III)-tetrakisphthalate framework for one-step adsorption-phase purification of C_2H_4 from C_2 hydrocarbons. *Inorg Chem.* 2021;60(14):10819-10829.

SUPPORTING INFORMATION

Additional supporting information can be found online in the Supporting Information section at the end of this article.

How to cite this article: Wu T, Yu C, Krishna R, et al. Porous materials with suitable pore size and dual-functional sites for benchmark one-step ethylene purification. *AIChE J.* 2024; 70(3):e18312. doi:10.1002/aic.18312